

Nonlinear Magnetics Model for Permanent Magnet Synchronous Machines Capturing Saturation and Temperature Effects

Kishan Srinivasan, *Student Member, IEEE*, Heath Hofmann, *Fellow, IEEE* and Jing Sun, *Fellow, IEEE*

Abstract—This paper proposes a nonlinear magnetics model for Permanent Magnet Synchronous Machines (PMSMs) that accurately captures the effects of magnetic saturation in the machine iron and variations in rotor temperature on the permanent magnet excitation. The proposed model considers the permanent magnet as a current source rather than the more commonly used flux-linkage source. A comparison of the two modelling approaches is conducted using Finite Element Analysis (FEA) for different machine designs as well as experimental validation, where it is shown that the proposed model has substantially better accuracy. The proposed model decouples magnetic saturation and rotor temperature effects in the current/flux-linkage relationship, allowing for adaptive estimation of the PM excitation.

Index Terms—Electric machine modeling, Permanent Magnet Synchronous Machines, Saturation Effects, Non-linear magnetics model.

I. INTRODUCTION

PERMANENT Magnet Synchronous Machines (PMSMs) have become the popular choice in applications such as vehicle electrification [1]–[9]. With recent advancements in cooling techniques, it is now possible to develop PMSM designs with very high operating current density, and hence power density [10]–[12]. At these high current excitation levels, PMSMs tend to exhibit significant nonlinear behavior due to saturation of their soft magnetic material. Furthermore, the remanent flux density of NdFeB permanent magnets (PMs) can decrease significantly with increasing rotor temperature [13]. References [14]–[19] demonstrate that both magnetic saturation and rotor temperature variation can significantly affect the magnetic properties of the machine, and hence its torque production capability. Thus, it is important to accurately capture these phenomena in machine models used for the purpose of control.

The most common controls model for PMSMs is the linear model, where flux-linkage/current relationship ($\vec{\lambda}^r$ - \vec{i}^r) in the rotor reference frame is modelled with an inductance matrix (\mathbf{L}) and a permanent magnet flux linkage source (Λ_{PM}) [20]–[22]. Rotor temperature variation is typically captured by modeling Λ_{PM} as a function of rotor temperature T_r . These models are inaccurate when the machine iron is magnetically saturated [22], [23].

$$\vec{\lambda}^r = \mathbf{L}\vec{i}^r + \vec{\lambda}_{pm}^r(T_r); \quad (1)$$

$$\mathbf{L} = \begin{bmatrix} L_d & 0 \\ 0 & L_q \end{bmatrix}, \quad \vec{\lambda}^r = \begin{bmatrix} \lambda_d^r \\ \lambda_q^r \end{bmatrix}, \quad \vec{i}^r = \begin{bmatrix} i_d^r \\ i_q^r \end{bmatrix},$$

$$\vec{\lambda}_{pm}^r(T_r) = \begin{bmatrix} \Lambda_{PM}(T_r) \\ 0 \end{bmatrix}. \quad (2)$$

Many different control-oriented models of PMSMs exist in the literature that attempt to model the nonlinear magnetic properties under certain assumptions [14]–[16], [23]–[37]. One of the assumptions that is typically made is to neglect the effects of temperature variation on the soft magnetic material properties, as permanent magnets are much more sensitive to temperature change due to their lower Curie temperature. The most common approach is to model the inductances [24], [26], [27], [30], [31], [33], [34] as a function of rotor reference frame currents i_d^r and i_q^r to capture the saturation phenomenon, while the permanent magnets (PMs) are modelled as a flux linkage source whose value varies with rotor temperature. However, this approach becomes inaccurate in regions of heavy saturation and significant rotor temperature variation [29]. A nonlinear model developed using the equivalent magnetic circuit approach is proposed in [35], but does not consider the effects of rotor temperature. Models have also been proposed [32], [36] that take into account saturation and cross saturation by using Look-Up Tables (LUTs). In an attempt to address issues with accuracy, [14], [15] propose forming higher-dimensional LUTs with current as a function of both flux linkage and rotor temperature, i.e. $\vec{i}^r = f(\vec{\lambda}^r, T_r)$. However, using this approach for real-time control requires measurement or estimation of the rotor temperature. Another approach is to calculate the inductance matrix as a function of rotor temperature and current from an N-dimensional LUT. A few authors [16], [37] have also suggested to include compensation terms to take into account rotor temperature variation in the LUT, which primarily captures saturation. All these different nonlinear models follow the similar premise of modeling the PM as a flux linkage source.

The last category of modeling approach involves using Finite Element Analysis (FEA) or reduced-order models formed using FEA [38]–[40]. However, these models are typically computationally intensive and hence not suitable for real-time control purposes. Moreover, obtaining accurate FEA models of actual PMSMs requires knowledge of the dimensional parameters and material properties of the machine, information which is not often available to the controls engineer.

An alternate approach is to model PM as a current source, as discussed in [8], [41], [42]. However, these are linear magnetic

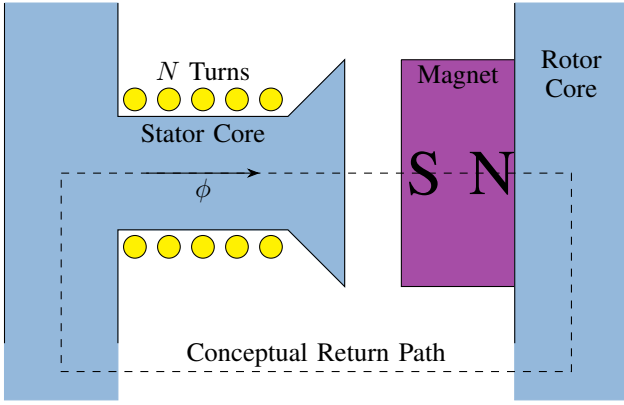


Fig. 1. Simplified, single-coil magnetics model of PMSM machine

models developed for simulation purposes and not for real-time control applications. In this paper, we present a magnetics model for PMSMs that accurately captures both the nonlinear and rotor-temperature-dependent behavior of PMSMs by modeling the PM as a current source as opposed the typical flux linkage source. A key contribution of this model is the decoupling of the nonlinear effects of magnetic saturation and the rotor temperature effect on permanent magnet excitation which is captured in a single parameter, the permanent magnet current. This parameter can then be adaptively estimated in real time, removing the need for measurement or estimation of the rotor temperature. The result is an accurate model suitable for use in real-time control.

The proposed PMSM model is introduced and justified in Section II. A comparison of the proposed model with a common nonlinear model is conducted using FEA simulation results for different machine designs is discussed in III-B. A similar comparison is conducted using experimental data in III-C, followed by concluding remarks in IV.

II. PROPOSED MODEL

A. Model development

The motivation for the proposed model is illustrated by considering the single-coil magnetic model shown in Fig. 2. We begin by creating a magnetic circuit model. The N -turn coil is represented by an magnetomotive force (MMF) source Ni , where i is the current flowing in the coil. The stator and rotor cores consist of a soft magnetic material exhibiting magnetic saturation, and so are represented by a nonlinear reluctance $\mathcal{R}_c(\phi)$ whose value varies with flux level ϕ . The PM is assumed to possess linear magnetic properties with an incremental permeability μ_m and a remanent flux density B_r that varies with rotor temperature T_r , and so is modeled as a constant reluctance \mathcal{R}_{pm} and flux source $\Phi_{pm}(T_r)$, as shown in Fig. 2.

An equivalent magnetic circuit can be created using the Thevenin equivalent of the PM, where the PM excitation is modelled as MMF source $F_{pm}(T_r) = \mathcal{R}_{pm}\Phi_{pm}(T_r)$ rather than a flux source. Simplifying the magnetic circuit further, the two reluctances are now in series and can be combined

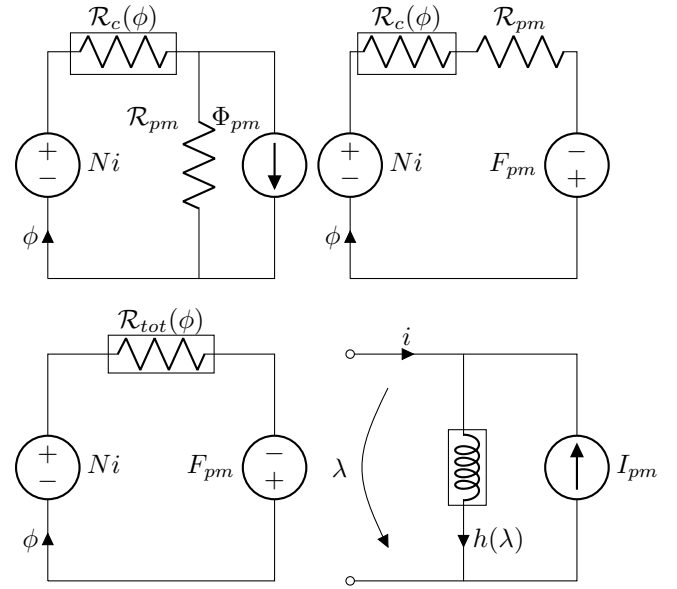


Fig. 2. Derivation of proposed magnetics model for single-coil. Top left: magnetic circuit model. Top right: Thevenin equivalent of permanent magnet. Bottom left: Combination of magnet and core reluctances. Bottom right: Resulting electric circuit model.

into a single nonlinear reluctance, $\mathcal{R}_{tot}(\phi)$. Analysis of the resulting magnetic circuit yields:

$$Ni + F_{pm}(T_r) = \mathcal{R}_{tot}(\phi)\phi = f(\phi) = f\left(\frac{\lambda}{N}\right); \quad (3)$$

$$\Rightarrow i = \frac{1}{N} \left(f\left(\frac{\lambda}{N}\right) - F_{pm}(T_r) \right) \quad (4)$$

$$= h(\lambda) - I_{pm}(T_r). \quad (5)$$

This expression can be represented in an electrical circuit model as a nonlinear inductance, with current/flux-linkage relationship $i = h(\lambda)$, in parallel with a current source $I_{pm}(T_r)$ representing the PM excitation, as shown in Fig. 2. As the value of I_{pm} is directly proportional to the remanent flux density B_r of the magnet, it will share the same dependence upon the rotor temperature.

In order to illustrate the advantages of the proposed model, we consider a model consisting of a nonlinear inductance and the more commonly used flux-linkage source representing permanent magnet excitation.

$$\lambda = \mathbf{L}(i)i + \Lambda_{pm}(T_r). \quad (6)$$

The key distinction between the two models is how the current/flux-linkage relationships react to changes in rotor temperature. In the case of the model (6) with a PM flux-linkage source, the result of a rotor temperature change would be a constant offset $\Delta\lambda$ in the $\lambda - i$ curve. In the case of the proposed model a change in rotor temperature would result in a constant offset ΔI .

Figure 3 shows a representative flux linkage/current relationship at two different rotor temperatures. One figure plots flux linkage versus current, the other current versus flux linkage. As can be seen, the variation of the $\lambda - i$ curve with temperature is not captured well by a constant offset in

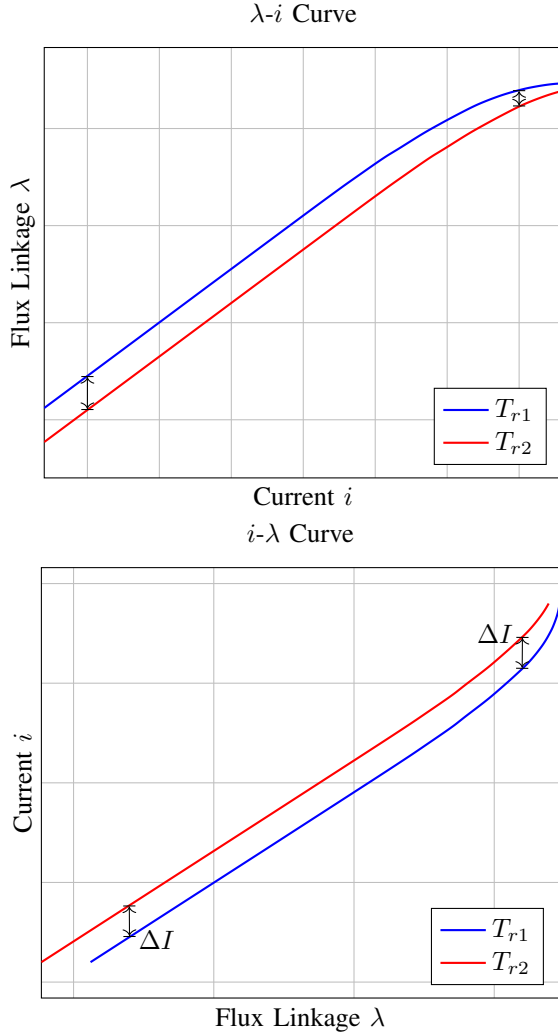


Fig. 3. Representative flux-linkage/current relationship capturing magnetic saturation at two different rotor temperatures. (a) $\lambda - i$ curve. (b) $i - \lambda$ curve.

the flux linkage. This is because the saturation effect results in a convergence of the flux linkage values at high current excitation. However, the variation of the $i - \lambda$ curve is well-captured by a constant offset in current.

B. Proposed Permanent Magnet Synchronous Machine Model

The proposed equivalent two-phase model for a Permanent Magnet Synchronous Machine (PMSM) is developed considering the standard smooth airgap model (i.e., effects due to the slots in the stator core are neglected).

1) *Current/flux-linkage relationship*: The current/flux-linkage relationships of the proposed machine model are presented in the rotor reference frame (designated by a superscript 'r'), which is related to the variables in the stationary reference frame as follows:

$$\vec{x}^r = e^{-\mathbf{J}\theta_{re}} \vec{x}, \quad \vec{x} = e^{\mathbf{J}\theta_{re}} \vec{x}^r. \quad (7)$$

where $\theta_{re} = \frac{N_p}{2}\theta_r$ is the electrical rotor angle,

$$\mathbf{J} = \begin{bmatrix} 0 & -1 \\ 1 & 0 \end{bmatrix}$$

is the 90° rotation matrix, N_p is the number of poles of the machine, and θ_r is the mechanical angle of the rotor. The matrix exponentials $e^{-\mathbf{J}\theta_{re}}$ and $e^{\mathbf{J}\theta_{re}}$ represents the Park and Inverse Park Transforms, respectively.

The current/flux-linkage relationships are an extension of the single-coil model discussed in the prequel to a vector representation:

$$\vec{i}^r = \vec{h}(\vec{\lambda}^r) - \vec{i}_{pm}^r(T_r) \quad (8)$$

or

$$\begin{bmatrix} i_d^r \\ i_q^r \end{bmatrix} = \begin{bmatrix} h_d(\lambda_d^r, \lambda_q^r) \\ h_q(\lambda_d^r, \lambda_q^r) \end{bmatrix} - \begin{bmatrix} I_{pm}(T_r) \\ 0 \end{bmatrix} \quad (9)$$

where I_{pm} represents the permanent magnet excitation.

The mapping $\vec{h}(\vec{\lambda}^r)$ captures the nonlinear effects of saturation of soft magnetic materials of the machine. and has the following property

$$\vec{h}(\vec{0}) = \vec{0}. \quad (10)$$

If the electric machine design has the standard symmetries, $\vec{h}(\vec{\lambda}^r)$ also has the following properties:

$$h_q(\lambda_d^r, -\lambda_q^r) = -h_q(\lambda_d^r, \lambda_q^r), \quad (11)$$

$$h_q(-\lambda_d^r, \lambda_q^r) = h_q(\lambda_d^r, \lambda_q^r), \quad (12)$$

$$h_d(\lambda_d^r, -\lambda_q^r) = h_d(\lambda_d^r, \lambda_q^r). \quad (13)$$

Assuming standard magnetic material properties (e.g., incremental permeabilities are always positive), it can be shown that $\vec{h}(\vec{\lambda}^r)$ is injective and surjective, and so an inverse flux-linkage/current relationship exists:

$$\vec{\lambda}^r = \vec{h}^{-1}(\vec{i}^r + \vec{i}_{pm}^r) = \vec{g}(\vec{i}^r + \vec{i}_{pm}^r). \quad (14)$$

2) *Stator voltage dynamic equations in rotor reference frame*: It can be shown that:

$$\vec{v}^r = R\vec{i}^r + \frac{N_{poles}}{2}\omega_r\mathbf{J}\vec{\lambda}^r + \frac{d\vec{\lambda}^r}{dt} \quad (15)$$

$$= R[\vec{h}(\vec{\lambda}^r) - \vec{i}_{pm}^r] + \frac{N_p}{2}\omega_r\mathbf{J}\vec{\lambda}^r + \frac{d\vec{\lambda}^r}{dt}, \quad (16)$$

where ω_r is the angular velocity of the rotor.

3) *Electromagnetic Torque*: To derive the torque expression, we begin with an expression for the stored magnetic field energy w_{fld} in a three-phase machine [43]. To simplify the analysis we leave out a (position-independent) energy component due to the magnets, which does not impact the final result.

$$\begin{aligned} w_{fld}(\vec{\lambda}, \theta_r) &= \frac{3}{2} \int_0^{\vec{\lambda}} \vec{i}^T(\vec{x}) d\vec{x} \\ &= \frac{3}{2} \int_0^{\vec{\lambda}} \left\{ e^{\mathbf{J}\theta_{re}} \left[\vec{h}(e^{-\mathbf{J}\theta_{re}} \vec{x}) - \vec{i}_{pm}^r \right] \right\}^T d\vec{x}. \end{aligned} \quad (17)$$

The electromagnetic torque can be shown to be:

$$\begin{aligned}\tau_{em} &= -\frac{\partial w_{fld}(\vec{\lambda}, \theta_r)}{\partial \theta_r} \\ &= \frac{3N_p}{4} \left[-(\vec{\lambda}^r)^T \mathbf{J} \vec{h}(\vec{\lambda}^r) + \vec{\lambda}^r \mathbf{J} \vec{i}_{pm}^r \right] \\ &= \frac{3N_p}{4} \left[h_q(\vec{\lambda}^r) \lambda_d^r - h_d(\vec{\lambda}^r) \lambda_q^r + I_{pm}(T_r) \lambda_q^r \right].\end{aligned}\quad (18)$$

The first term in (18) corresponds to a (nonlinear) reluctance torque and the second term is the PM torque.

III. VALIDATION AND COMPARISON RESULTS

In this section we will illustrate the accuracy of the proposed model through comparison with a baseline PM flux-linkage model. We will first introduce the baseline model. We will then compare how changes in the rotor temperature affect the accuracy of the proposed and baseline models. The first comparisons will be conducted using FEA results for three different machine designs: an interior permanent machine, a distributed-winding surface mount permanent magnet (SMPM) machine, and a concentrated-winding SMPM machine. Finally, a comparison will be conducted using experimental results.

A. Baseline model

We will use the following nonlinear PM flux linkage model from literature [33] as a baseline for comparison with the proposed model:

$$\vec{\lambda}^r = \mathbf{L}(\vec{i}^r) \vec{i}^r + \vec{\lambda}_{pm}^r(T_r), \quad (19)$$

$$\mathbf{L}(\vec{i}^r) = \begin{bmatrix} L_d(i_d^r) & L_{dq}(i_d^r, i_q^r) \\ L_{qd}(i_d^r, i_q^r) & L_q(i_q^r) \end{bmatrix}, \quad (20)$$

$$\vec{\lambda}_{pm}^r(T_r) = \begin{bmatrix} \Lambda_{PM}(T_r) \\ 0 \end{bmatrix}$$

where,

$$\begin{aligned}L_d(i_d^r) &= \frac{\lambda_d^r(i_d^r, 0) - \Lambda_{pm}(T_r)}{i_d^r}, \\ L_q(i_q^r) &= \frac{\lambda_q^r(0, i_q^r)}{i_q^r}, \\ L_{dq}(i_d^r, i_q^r) &= \frac{\lambda_d^r(i_d^r, 0) - \lambda_d^r(i_d^r, i_q^r)}{i_q^r}, \\ L_{qd}(i_d^r, i_q^r) &= \frac{\lambda_q^r(0, i_q^r) - \lambda_q^r(i_d^r, i_q^r)}{i_d^r}\end{aligned}$$

and the torque is given by

$$\begin{aligned}\tau_{em} &= \frac{3N_p}{4} \left[L_{dq}(i_d^r, i_q^r) (i_q^r)^2 + (L_d(i_d^r) - L_q(i_q^r)) i_d^r i_q^r + \right. \\ &\quad \left. \Lambda_{pm}(T_r) i_q^r - L_{qd}(i_d^r, i_q^r) (i_d^r)^2 \right].\end{aligned}\quad (21)$$

This particular model was chosen as it separates the nonlinear behavior from a rotor-temperature-dependent parameter ($\Lambda_{pm}(T_r)$), the same as the proposed NL PM current model.

B. Model comparison using FEA-based data

We first use two-dimensional finite element analysis (FEA) results from ANSYS as the basis for comparison. The process that is used to compare the two models is as follows:

- 1) Using FEA, calculate the flux linkages λ_d^r and λ_q^r and the electromagnetic torque τ_{em} over a range of currents i_d^r and i_q^r with the rotor temperature set at $T_1 = 60^\circ\text{C}$.
- 2) Use the flux-linkage/current data to determine the values of $I_{pm}(T_1)$ (used in the proposed model) and $\Lambda_{pm}(T_1)$ (used in the baseline model). The value of Λ_{pm} is determined from λ_d^r by setting the currents to zero, and the value of I_{pm} is determined by finding the value of i_d^r that sets $\lambda_d^r = 0$.
- 3) Generate a look-up table for the $\vec{\lambda}^r = \vec{g}(\vec{i}^r + \vec{i}_{pm}^r)$ mapping of the proposed model using 60°C FEA data. Note that we determine the $\vec{g}(\circ)$ mapping rather than the $\vec{h}(\circ)$ mapping to better enable the comparison.
- 4) Generate a look-up table for the inductances in (20) for the baseline model using the 60°C FEA data.
- 5) Repeat steps 1) and 2) for a different rotor temperature (T_2).
- 6) Compute the flux linkages and torques with the proposed model using the nonlinear look-up table for $\vec{g}(\cdot)$ determined from the T_1 data and $I_{pm}(T_2)$ for the proposed model.
- 7) Compute the flux linkages and torques with the comparison model using the nonlinear look-up table $\mathbf{L}(\cdot)$ from the T_1 data and $\Lambda_{pm}(T_2)$ for the baseline model.
- 8) Compare the results from the previous steps 6) and 7) with the FEA results at the new rotor temperature (T_2).

1) *Interior permanent magnet machine:* We first consider the interior permanent magnet machine design presented in [44] and shown in Fig. 4. The permanent magnet material

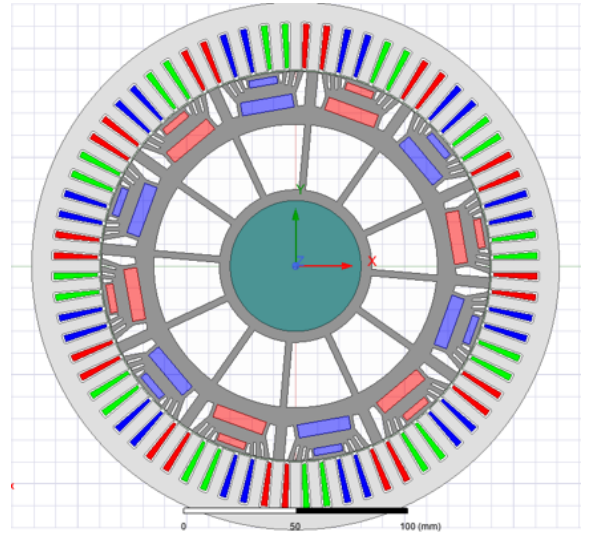


Fig. 4. Cross-section of Interior Permanent Magnet machine [44]

used is NdFeB N35UH from Arnold Magnetics [13]. The mechanical dimensions and winding parameters are kept the same as in [44]. With the recent advancements in cooling mechanisms as shared in [45], peak current densities of $48 \text{ A}_{rms}/\text{mm}^2$ can be achieved. We use this value to determine

the maximum current of the mapping, though we note that this machine was not specifically designed for these current densities.

The NL $\vec{\lambda}^r - \vec{i}^r$ mapping, determined using FEA at temperatures $T_1=60^\circ C$ and $T_2=100^\circ C$, is shown in Fig. 5. As is

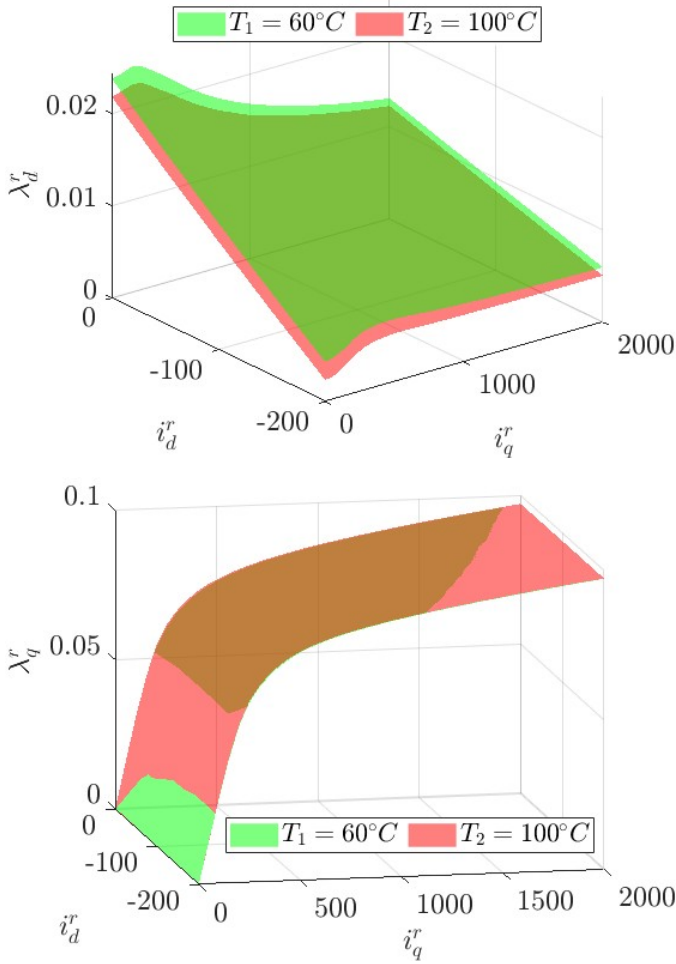


Fig. 5. $\vec{\lambda}^r - \vec{i}^r$ mapping of interior permanent magnet machine at different rotor temperatures

to be expected, we see a significant change in λ_d^r whereas λ_q^r is not substantially different. The value of I_{pm} and Λ_{pm} was determined for multiple temperatures and is shown in Table. I.

TABLE I
 I_{pm} AND Λ_{pm} VALUES FOR INTERIOR PERMANENT MAGNET MACHINE

Temperature ($^\circ C$)	I_{pm} (A)	Λ_{pm} (V - s)
20	264.8	0.0256
60	245.6	0.0238
80	235.1	0.0227
100	225.4	0.0219

The absolute errors in λ_d^r and λ_q^r for both the proposed PM current model and the baseline PM flux linkage model are shown in Figs. 6 - 7. It can be seen that the baseline PM flux linkage model experiences significantly larger error in λ_d^r at

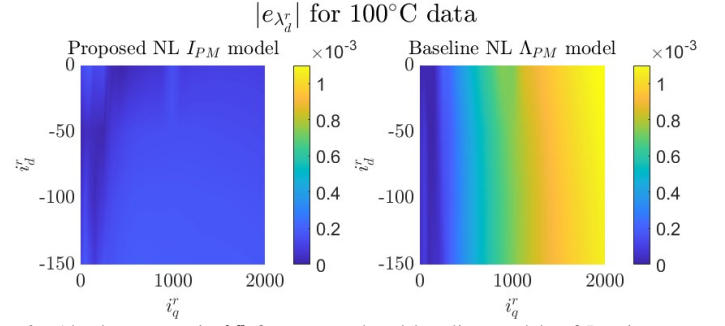


Fig. 6. Absolute errors in λ_d^r for proposed and baseline models of Interior Permanent Magnet machine when compared to FEA results.

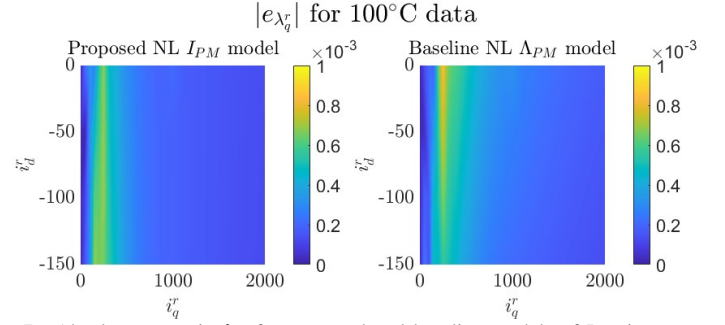


Fig. 7. Absolute errors in λ_q^r for proposed and baseline models of Interior Permanent Magnet machine when compared to FEA results.

high values of i_q^r when compared to the proposed PM current model. In the case of λ_q^r , the model errors are similar, and occur at the onset of magnetic saturation on the quadrature axis.

The relative error in torque for the two models is highlighted in Fig. 8. It can be clearly seen that the proposed PM current

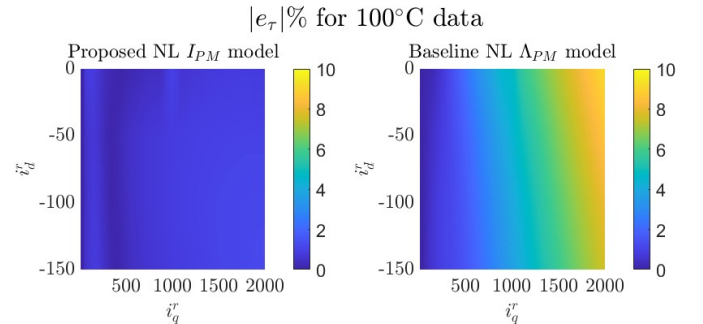


Fig. 8. Relative errors in torque for proposed and baseline models of Interior Permanent Magnet machine when compared to FEA results.

model shows a significant improvement in torque accuracy when compared to the PM flux linkage model, especially at high values of i_q^r when the machine iron is heavily saturated.

2) *Distributed-winding SMPM machine*: A 4 pole, distributed winding SMPM (Fig. 9) with machine parameters as shown in Table. VI is simulated in ANSYS FEA for rotor temperatures $T_1 = 60^\circ C$ and $T_2 = 120^\circ C$. The machine is simulated with current density of $13 A_{rms}/mm^2$, which corresponds to forced-air cooling conditions. It can be seen that the proposed PM current model outperforms the PM flux linkage model. Values of I_{pm} and Λ_{pm} for different rotor temperatures are provided in Table. III for this machine design.

TABLE II
DISTRIBUTED WINDING SMPM PARAMETERS

Parameter	Value
Number of poles	4
Number of slots	24
Conductors per slot	100
Parallel branches	1
Magnet material	NdFe35 (N35UH)
Steel type	M19 24G
Stator outer diameter (mm)	160
Stator inner diameter (mm)	80
Rotor outer diameter (mm)	78
Magnet thickness (mm)	5
Machine length (mm)	80

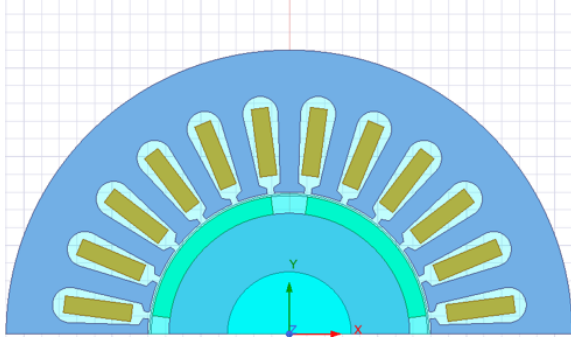


Fig. 9. Cross-section of Distributed winding SMPM machine in ANSYS Maxwell

Figs 10 through 12 show absolute errors in λ_d^r and λ_q^r and the

TABLE III
 I_{pm} AND Λ_{pm} VALUES FOR DISTRIBUTED WINDING SMPM MACHINE

Temperature ($^{\circ}C$)	I_{pm} (A)	$\Lambda_{pm}(V - s)$
60	38.4	1.2281
80	37.3	1.2048
100	36.3	1.1842
120	35.1	1.156

relative torque error for the two models at temperature T_2 . It can be seen that, for λ_d^r and hence torque, significant errors occur for negative values of i_d^r . This is due to the fact that the machine iron is saturated by the permanent magnets at zero current excitation. The field-weakening effect of negative i_d^r drives the iron out of saturation and so causes the effective PM flux linkage to increase, resulting in the error.

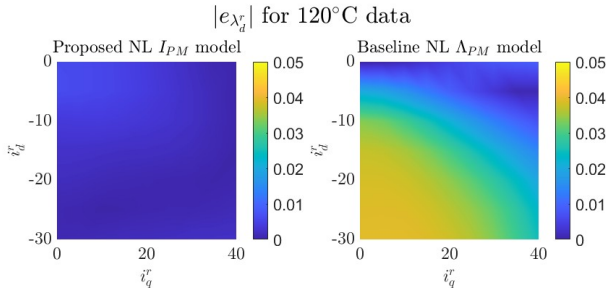


Fig. 10. Absolute errors in λ_d^r for proposed and baseline models of distributed winding SMPM

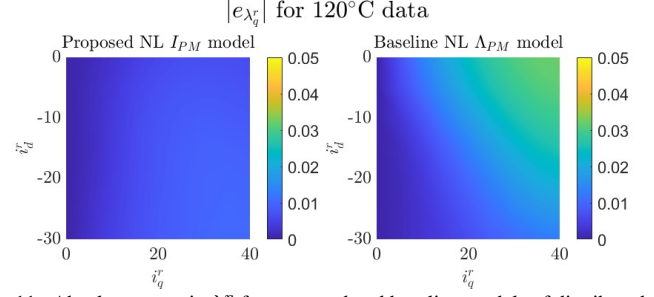


Fig. 11. Absolute errors in λ_q^r for proposed and baseline models of distributed winding SMPM

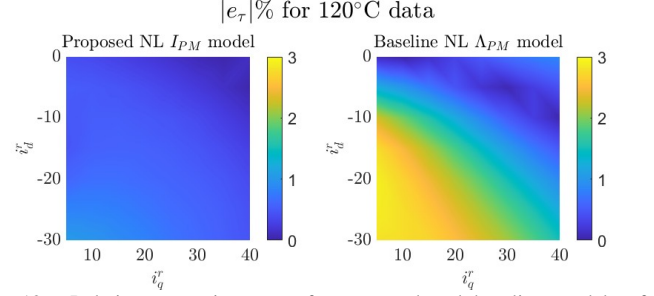


Fig. 12. Relative errors in torque for proposed and baseline models of distributed winding SMPM

3) *Concentrated-winding SMPM machine*: A simple 4-pole concentrated winding SMPM with machine parameters as shown in Table. IV is simulated in ANSYS FEA for rotor temperatures $T_1 = 60^{\circ}C$ and $T_2 = 100^{\circ}C$. The machine is simulated with a peak current density of $31 A_{rms}/mm^2$, corresponding to liquid cooling conditions. The machine cross section is shown in Fig. 13. The I_{pm} and Λ_{pm} values for this

TABLE IV
CONCENTRATED WINDING SMPM PARAMETERS

Parameter	Value
Number of poles	4
Number of slots	6
Conductors per slot	220
Parallel branches	1
Magnet material	NdFe35 (N35UH)
Steel type	M19 24G
Stator outer diameter (mm)	220
Stator inner diameter (mm)	80
Rotor outer diameter (mm)	74
Magnet thickness (mm)	3
Machine length (mm)	80

machine is shown in Table. V. The absolute error in λ_d^r and λ_q^r

TABLE V
 I_{pm} AND Λ_{pm} VALUES FOR CONCENTRATED WINDING SMPM MACHINE

Temperature ($^{\circ}C$)	I_{pm} (A)	$\Lambda_{pm}(V - s)$
20	25.8	0.399
60	24.6	0.3813
80	23.9	0.3701
100	23.3	0.3609
120	22.5	0.3491

for both models is compared as shown in Figs. 14-15. Relative error in estimated torque by both models is compared in Fig.

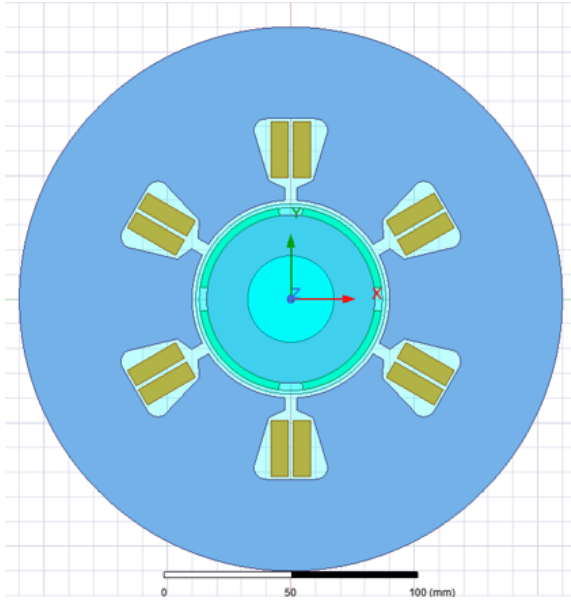


Fig. 13. Cross-section of concentrated winding SMPM machine in ANSYS Maxwell

16. We can clearly observe the improvement in accuracy in the proposed model from Figs 14 and 16, especially in the region of high torque where magnetic saturation is most prominent.

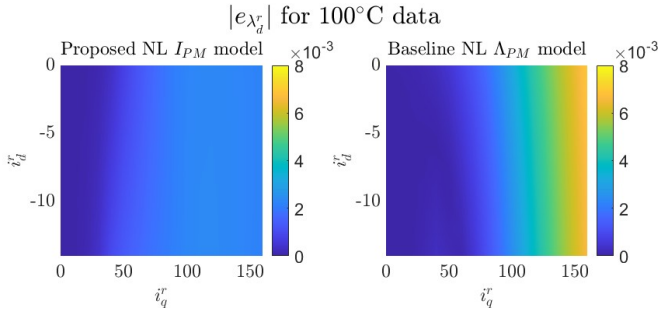


Fig. 14. Absolute errors in λ_d^r for proposed and baseline models of concentrated winding SMPM

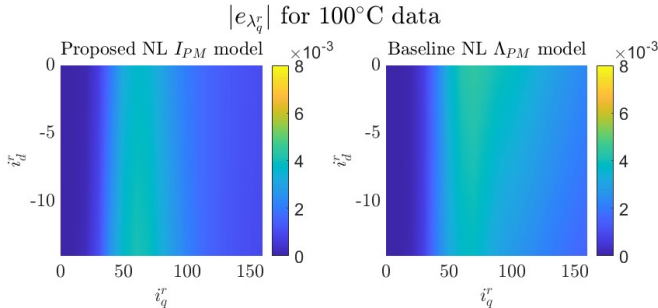


Fig. 15. Absolute errors in λ_q^r for proposed and baseline models of concentrated winding SMPM

C. Experimental Validation

1) *Setup*: A three phase, 18 pole, 145kW UQM SMPM with specifications as shown in Table VI is characterized using

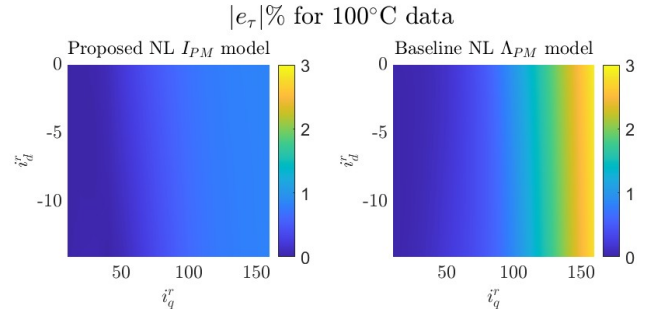


Fig. 16. Relative errors in torque for proposed and baseline models of concentrated winding SMPM

a dSpace Scalexio real-time target controller that uses auto-generated code from MATLAB/Simulink. A 3 phase voltage source inverter consisting of SKiiP 1814 GB17E4-3DUW V2 IGBTs, made by Semikron, is used with a switching frequency of 10 kHz, bus voltage of 175 V, and dead-time of 2 μ s. Space-Vector Modulation (SVM) is used as the modulation scheme to calculate the desired duty-cycles. The rotor speed is kept constant at 500rpm by an electric-machine-based dynamometer. This speed was chosen as the voltage/current relationships of the machine are relatively insensitive to both winding resistance and core losses at the corresponding electrical frequency (75Hz). An infrared temperature sensor from Texense (IRN2) is used to measure and maintain the rotor temperature to constant. Since it is difficult to keep the rotor temperature constant, efforts were made to collect data quickly to keep the temperature variation within 5°C. The experimental setup of the hardware is shown in Fig. 17. The SMPM test flux-

TABLE VI
TEST MACHINE RATING

Description	Value
Number of poles	18
Manufacturer	UQM Technologies
Type	PM Brushless
Maximum speed	8000rpm
Maximum Current	500A
Maximum Voltage	450V
Rated Power	145KW peak/ 85 KW continuous

linkage/current relationship was characterized using a process similar to that provided in [46], [47], where flux linkage is estimated by numerically integrating the electromotive force (emf) of the stator windings. The machine under test does not experience appreciable saturation under normal operation. Therefore, to illustrate the benefits of the proposed model, operating points with positive values of i_d^r were used in order to bring the machine iron into magnetic saturation. To simplify testing the current i_q^r was set to zero and i_d^r was varied from -300A to 500A. The resulting $\lambda_d^r - i_d^r$ relationships are shown in Fig. 18 for rotor temperatures $T_1 = 60^\circ C$ and $T_2 = 90^\circ C$.

2) *Calculation of I_{pm} and Λ_{pm}* : The $\lambda_d^r - i_d^r$ characterization process used does not provide accurate flux-linkage estimates with high levels of field weakening (i.e., negative values of i_d^r .) This is due to the fact that, in these circumstances, the emf of the windings becomes a small fraction of the overall

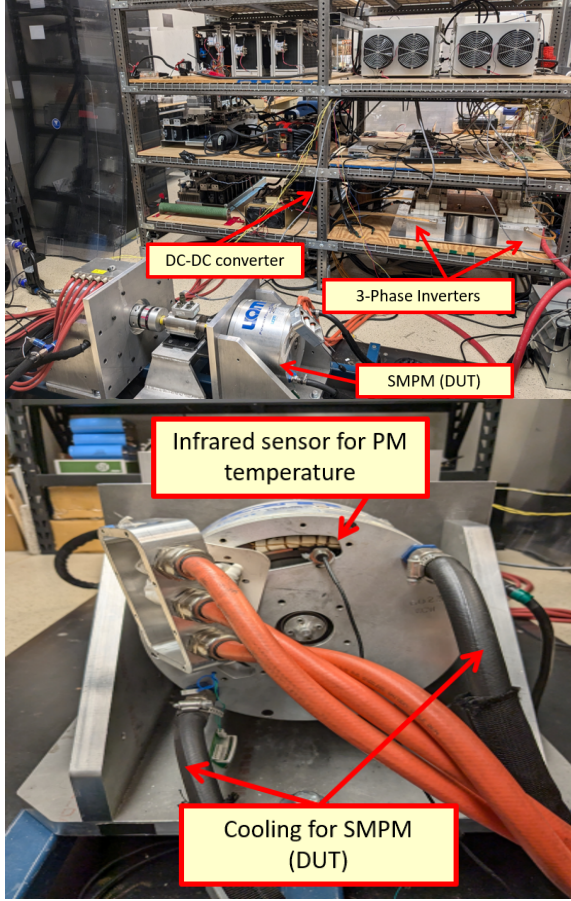


Fig. 17. (a) Hardware setup for experiment, (b) Infrared sensor for rotor temperature measurement on the SMPM test machine

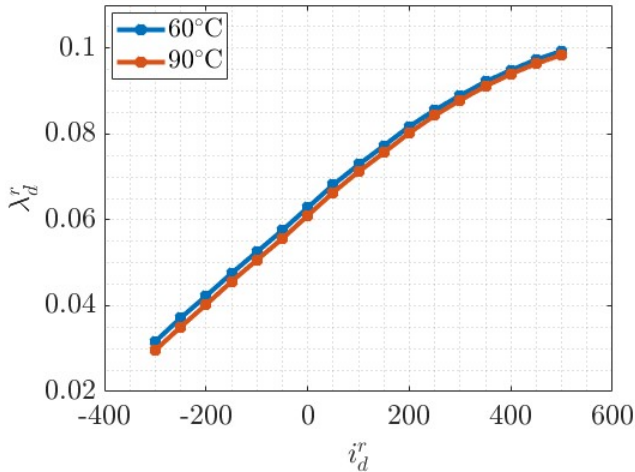


Fig. 18. Experimental $\lambda_d^r - i_d^r$ characterization of UQM 145 machine for rotor temperatures $T_1 = 60^\circ C$ and $T_2 = 90^\circ C$, $i_q^r = 0$.

voltage. As a result, the estimated flux linkages become highly sensitive to errors in the estimated winding resistance and voltage drops of the inverter transistors, which are used to calculate the emf. Hence we cannot accurately determine the zero-flux-linkage condition as we did with the FEA results, and so another method must be used to determine the value of I_{pm} . This is achieved through the following process:

- Using the experimentally determined $\lambda_d^r - i_d^r$ data at temperature T_1 , create a function which calculates $\lambda_d^r = g_{dT_1}(i_d^r + I_{pmT_1})$ for a given value of I_{pmT_1} through the use of lookup tables and linear interpolation.
- Repeat the above step for data taken at temperature T_2 .
- Determine the values of I_{pm} at temperatures T_1 and T_2 simultaneously by solving the following minimization problem

$$\min_{I_{pmT_1}, I_{pmT_2}} \|g_{dT_1}(i_d^r + I_{pmT_1}) - g_{dT_2}(i_d^r + I_{pmT_2})\|^2, \quad (22)$$

where $\|\cdot\|$ represents the L^2 norm.

For the baseline NL PM flux linkage model, Λ_{pm} is computed from the experimental through two different methods as described below.

Method 1: This is same method described earlier in III-B where Λ_{pm} is determined from the estimated λ_d^r when the currents to zero.

Method 2: This method is analogous to the one used to compute I_{pm} . Functions $f_{dT_1}(\lambda_d^r - \Lambda_{pmT_1})$ and $f_{dT_2}(\lambda_d^r - \Lambda_{pmT_2})$ are constructed for given values of Λ_{pmT_1} and Λ_{pmT_2} using the experimental data taken at temperatures T_1 and T_2 , respectively. The values of the PM flux linkage at temperatures T_1 and T_2 are then determined simultaneously by solving the following minimization problem

$$\min_{\Lambda_{pmT_1}, \Lambda_{pmT_2}} \|f_{dT_1}(\lambda_d^r - \Lambda_{pmT_1}) - f_{dT_2}(\lambda_d^r - \Lambda_{pmT_2})\|^2. \quad (23)$$

The solver `fmincon` in MATLAB was used to solve the optimization problems to compute I_{pm} and Λ_{pm} . The values of I_{pm} and Λ_{pm} for both rotor temperatures ($T_1 = 60^\circ C$ and $T_2 = 90^\circ C$) from experimental results is shown in Table. VII.

TABLE VII
EXPERIMENTAL I_{pm} AND Λ_{pm} VALUES

Temperature ($^\circ C$)	I_{pm} (A)	Λ_{pm} (V-s)	
		Method 1	Method 2
60	603.6	0.0628	0.0625
90	585.4	0.0610	0.0609

3) **Comparison results:** The models were compared using the same technique used in III-B for the FEA results. Fig. 19 shows the absolute error in λ_d^r for the NL PM current model and NL PM flux linkage model, where the value of Λ_{pm} for the NL PM flux linkage model at temperature T_2 was computed using Method 1. While the models show similar accuracy in the linear region (i.e., negative i_d^r excitation), one can distinctly observe the improved accuracy of the proposed model in the

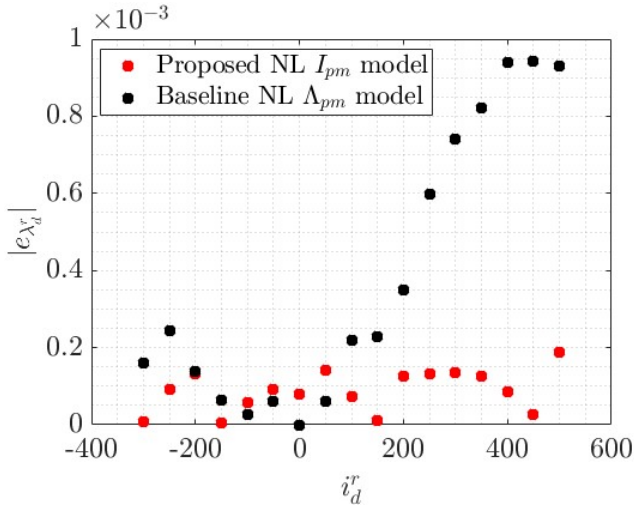


Fig. 19. Absolute errors in λ_d^r for proposed NL PM current and baseline NL PM flux linkage models at 90°C using Method 1 for Λ_{pm} calculation

region of magnetic saturation. Fig. 20 compares the absolute error in λ_d^r when Λ_{pm} for the NL PM flux linkage model is computed using Method 2. In this case, the proposed model shows better accuracy in both the nonlinear and linear regions.

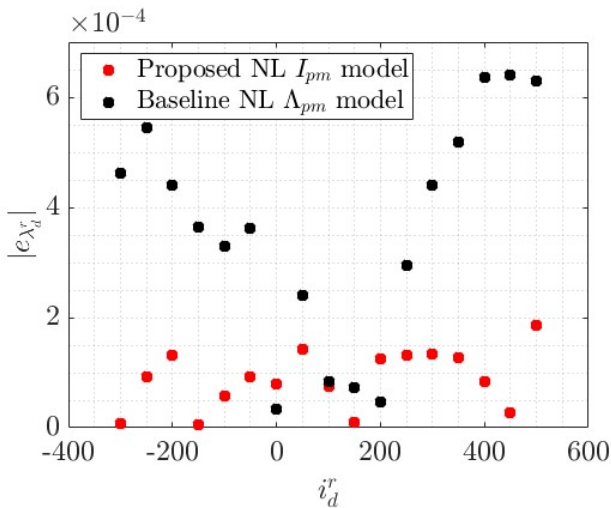


Fig. 20. Absolute errors in λ_d^r for proposed NL PM current and baseline NL PM flux linkage models at 90°C using Method 2 for Λ_{pm} calculation

IV. CONCLUSION

A machine model for PMSMs that captures the effects of magnetic saturation and rotor temperature variations has been proposed that is accurate and computationally inexpensive, and so can be utilized in real time control applications. The main contribution of the proposed model is the decoupling of the effects of magnetic saturation and rotor temperature variation, the latter being captured in a PM current parameter I_{pm} . This parameter can be adaptively estimated, thereby avoiding the need for rotor temperature measurement. The proposed model is validated using FEA simulation for an interior permanent magnet machine design, a distributed winding SMPM design, and a concentrated winding SMPM design, and shows high

accuracy at different rotor temperatures when compared with a nonlinear PM flux linkage model. Experimental results also show that the proposed model is more accurate than the nonlinear PM flux linkage model.

Future work will involve the development of a torque regulator algorithm, including an adaptive estimator for PM current, that is based upon the proposed model.

V. ACKNOWLEDGEMENTS

This material is based on work supported by the Office of Naval Research under Grant No.: N000-14-18-1-2330.

REFERENCES

- [1] C. C. Chan, "The state of the art of electric, hybrid, and fuel cell vehicles," *Proceedings of the IEEE*, vol. 95, no. 4, pp. 704–718, 2007.
- [2] Z. Yang, F. Shang, I. P. Brown, and M. Krishnamurthy, "Comparative study of interior permanent magnet, induction, and switched reluctance motor drives for ev and hev applications," *IEEE Transactions on Transportation Electrification*, vol. 1, no. 3, pp. 245–254, 2015.
- [3] G. Pellegrino, A. Vagati, P. Guglielmi, and B. Boazzo, "Performance comparison between surface-mounted and interior pm motor drives for electric vehicle application," *IEEE Transactions on Industrial Electronics*, vol. 59, no. 2, pp. 803–811, 2012.
- [4] B. Bilgin, P. Magne, P. Malysz, Y. Yang, V. Pantelic, M. Preindl, A. Korobkine, W. Jiang, M. Lawford, and A. Emadi, "Making the case for electrified transportation," *IEEE Transactions on Transportation Electrification*, vol. 1, no. 1, pp. 4–17, 2015.
- [5] J. Weimer, "The role of electric machines and drives in the more electric aircraft," in *IEEE International Electric Machines and Drives Conference, 2003. IEMDC'03.*, vol. 1, 2003, pp. 11–15 vol.1.
- [6] R. Krishnan and A. Bharadwaj, "A comparative study of various motor drive systems for aircraft applications," in *Conference Record of the 1991 IEEE Industry Applications Society Annual Meeting*, 1991, pp. 252–258 vol.1.
- [7] B. Sarlioglu and C. T. Morris, "More electric aircraft: Review, challenges, and opportunities for commercial transport aircraft," *IEEE Transactions on Transportation Electrification*, vol. 1, no. 1, pp. 54–64, 2015.
- [8] T. M. Jahns, G. B. Kliman, and T. W. Neumann, "Interior permanent-magnet synchronous motors for adjustable-speed drives," *IEEE Transactions on Industry Applications*, vol. IA-22, no. 4, pp. 738–747, 1986.
- [9] P. B. Reddy, A. El-Refaeie, K.-K. Huh, J. K. Tangudu, and T. M. Jahns, "Comparison of interior and surface pm machines equipped with fractional-slot concentrated windings for hybrid traction applications," in *2011 IEEE Energy Conversion Congress and Exposition*, 2011, pp. 2252–2259.
- [10] A. Tüysüz, F. Meyer, M. Steichen, C. Zwysig, and J. W. Kolar, "Advanced cooling methods for high-speed electrical machines," *IEEE Transactions on Industry Applications*, vol. 53, no. 3, pp. 2077–2087, 2017.
- [11] D. Lee, T. Balachandran, S. Sirimanna, N. Salk, A. Yoon, P. Xiao, J. Macks, Y. Yu, S. Lin, J. Schuh, P. Powell, and K. S. Haran, "Detailed design and prototyping of a high power density slotless pmsm," *IEEE Transactions on Industry Applications*, vol. 59, no. 2, pp. 1719–1727, 2023.
- [12] A. M. El-Refaeie, J. P. Alexander, S. Galioto, P. Reddy, K.-K. Huh, P. de Bock, and X. Shen, "Advanced high power-density interior permanent magnet motor for traction applications," in *2013 IEEE Energy Conversion Congress and Exposition*, 2013, pp. 581–590.
- [13] *Sintered Neodymium-Iron-Boron Magnets*, Arnold Magnetic Technologies, rev. 210607. [Online]. Available: <https://www.arnoldmagnetics.com/wp-content/uploads/2017/11/N35UH-151021.pdf>
- [14] S. Li, B. Sarlioglu, S. Jurkovic, N. R. Patel, and P. Savagian, "Analysis of temperature effects on performance of interior permanent magnet machines for high variable temperature applications," *IEEE Transactions on Industry Applications*, vol. 53, no. 5, pp. 4923–4933, 2017.
- [15] —, "Comparative analysis of torque compensation control algorithms of interior permanent magnet machines for automotive applications considering the effects of temperature variation," *IEEE Transactions on Transportation Electrification*, vol. 3, no. 3, pp. 668–681, 2017.
- [16] S. Li, D. Han, and B. Sarlioglu, "Modeling of interior permanent magnet machine considering saturation, cross coupling, spatial harmonics, and

- temperature effects,” *IEEE Transactions on Transportation Electrification*, vol. 3, no. 3, pp. 682–693, 2017.
- [17] I. Voncilă, I. Paraschiv, and M. Costin, “The influence of saturation on the performance of pmsm,” in *2021 7th International Symposium on Electrical and Electronics Engineering (ISEEE)*, 2021, pp. 1–6.
- [18] T. Sebastian, “Temperature effects on torque production and efficiency of pm motors using ndfeb magnets,” *IEEE Transactions on Industry Applications*, vol. 31, no. 2, pp. 353–357, 1995.
- [19] Y.-S. Kim and S.-K. Sul, “Torque control strategy of an ipmsm considering the flux variation of the permanent magnet,” pp. 1301–1307, 2007.
- [20] P. Pillay and R. Krishnan, “Modeling of permanent magnet motor drives,” *IEEE Transactions on Industrial Electronics*, vol. 35, no. 4, pp. 537–541, 1988.
- [21] —, “Modeling, simulation, and analysis of permanent-magnet motor drives. i. the permanent-magnet synchronous motor drive,” *IEEE Transactions on Industry Applications*, vol. 25, no. 2, pp. 265–273, 1989.
- [22] T. Sebastian, G. Slemon, and M. Rahman, “Modelling of permanent magnet synchronous motors,” *IEEE Transactions on Magnetics*, vol. 22, no. 5, pp. 1069–1071, 1986.
- [23] F. Parasiliti and P. Poffet, “A model for saturation effects in high-field permanent magnet synchronous motors,” *IEEE Transactions on Energy Conversion*, vol. 4, no. 3, pp. 487–494, 1989.
- [24] S. L. Kellner and B. Piepenbreier, “General pmsm d,q-model using optimized interpolated absolute and differential inductance surfaces,” in *2011 IEEE International Electric Machines & Drives Conference (IEMDC)*, 2011, pp. 212–217.
- [25] G. Luo, R. Zhang, Z. Chen, W. Tu, S. Zhang, and R. Kennel, “A novel nonlinear modeling method for permanent-magnet synchronous motors,” *IEEE Transactions on Industrial Electronics*, vol. 63, no. 10, pp. 6490–6498, 2016.
- [26] X. Sun and X. Xiao, “Precise non-linear flux linkage model for permanent magnet synchronous motors based on current injection and bivariate function approximation,” *IET Electric Power Applications*, vol. 14, no. 11, pp. 2044–2050.
- [27] K. Drobnič, L. Gašparin, and R. Fišer, “Fast and accurate model of interior permanent-magnet machine for dynamic characterization,” *Energies*, vol. 12, no. 5, 2019. [Online]. Available: <https://www.mdpi.com/1996-1073/12/5/783>
- [28] C. Choi, W. Lee, S.-O. Kwon, and J.-P. Hong, “Experimental estimation of inductance for interior permanent magnet synchronous machine considering temperature distribution,” *IEEE Transactions on Magnetics*, vol. 49, no. 6, pp. 2990–2996, 2013.
- [29] K. Rahman and S. Hiti, “Identification of machine parameters of a synchronous motor,” *IEEE Transactions on Industry Applications*, vol. 41, no. 2, pp. 557–565, 2005.
- [30] B. Stumberger, G. Stumberger, D. Dolinar, A. Hamler, and M. Trlep, “Evaluation of saturation and cross-magnetization effects in interior permanent-magnet synchronous motor,” *IEEE Transactions on Industry Applications*, vol. 39, no. 5, pp. 1264–1271, 2003.
- [31] N. Bianchi and S. Bolognani, “Magnetic models of saturated interior permanent magnet motors based on finite element analysis,” in *Conference Record of 1998 IEEE Industry Applications Conference. Thirty-Third IAS Annual Meeting (Cat. No.98CH36242)*, vol. 1, 1998, pp. 27–34 vol.1.
- [32] D. Hu, Y. M. Alsmadi, and L. Xu, “High-fidelity nonlinear ipm modeling based on measured stator winding flux linkage,” *IEEE Transactions on Industry Applications*, vol. 51, no. 4, pp. 3012–3019, 2015.
- [33] J. G. Cintron-Rivera, A. S. Babel, E. E. Montalvo-Ortiz, S. N. Foster, and E. G. Strangas, “A simplified characterization method including saturation effects for permanent magnet machines,” in *2012 XXth International Conference on Electrical Machines*, 2012, pp. 837–843.
- [34] T. Herold, D. Franck, E. Lange, and K. Hameyer, “Extension of a d-q model of a permanent magnet excited synchronous machine by including saturation, cross-coupling and slotting effects,” in *2011 IEEE International Electric Machines & Drives Conference (IEMDC)*, 2011, pp. 1363–1367.
- [35] K. J. Meessen, P. Thelin, J. Soulard, and E. A. Lomonova, “Inductance calculations of permanent-magnet synchronous machines including flux change and self- and cross-saturations,” *IEEE Transactions on Magnetics*, vol. 44, no. 10, pp. 2324–2331, 2008.
- [36] X. Chen, J. Wang, B. Sen, P. Lazari, and T. Sun, “A high-fidelity and computationally efficient model for interior permanent-magnet machines considering the magnetic saturation, spatial harmonics, and iron loss effect,” *IEEE Transactions on Industrial Electronics*, vol. 62, no. 7, pp. 4044–4055, 2015.
- [37] X. Chen, J. Wang, and A. Griffio, “A high-fidelity and computationally efficient electrothermally coupled model for interior permanent-magnet machines in electric vehicle traction applications,” *IEEE Transactions on Transportation Electrification*, vol. 1, no. 4, pp. 336–347, 2015.
- [38] S. Lin, X. Li, T. Wu, L. Chow, Z. Tang, and S. Stanton, “Temperature dependent reduced order ipm motor model based on finite element analysis,” in *2015 IEEE International Electric Machines & Drives Conference (IEMDC)*, 2015, pp. 543–549.
- [39] F. Poltschak and W. Amrhein, “A dynamic nonlinear model for permanent magnet synchronous machines,” in *2008 IEEE International Symposium on Industrial Electronics*, 2008, pp. 724–729.
- [40] H. Cai and D. Hu, “On pmsm model fidelity and its implementation in simulation,” in *2018 IEEE Energy Conversion Congress and Exposition (ECCE)*, 2018, pp. 1674–1681.
- [41] T. Sebastian and G. Slemon, “Transient modeling and performance of variable-speed permanent-magnet motors,” *IEEE Transactions on Industry Applications*, vol. 25, no. 1, pp. 101–106, 1989.
- [42] A. B. Dehkordi, A. Gole, and T. Maguire, “Permanent magnet synchronous machine model for real-time simulation,” 2005. [Online]. Available: <https://api.semanticscholar.org/CorpusID:15953835>
- [43] A. E. Fitzgerald, C. Kingsley, and S. D. Umans, *Electric Machinery*. McGraw-Hill, 2014.
- [44] M. Gierczynski and L. M. Grzesiak, “Comparative analysis of the steady-state model including non-linear flux linkage surfaces and the simplified linearized model when applied to a highly-saturated permanent magnet synchronous machine—evaluation based on the example of the bmw i3 traction motor,” *Energies*, vol. 14, no. 9, 2021. [Online]. Available: <https://www.mdpi.com/1996-1073/14/9/2343>
- [45] P. Alvarez, M. Satrustegui, I. Elósegui, and M. Martínez-Iturralde, “Review of high power and high voltage electric motors for single-aisle regional aircraft,” *IEEE Access*, vol. 10, pp. 112 989–113 004, 2022.
- [46] E. Armando, R. I. Bojoi, P. Guglielmi, G. Pellegrino, and M. Pastorelli, “Experimental identification of the magnetic model of synchronous machines,” *IEEE Transactions on Industry Applications*, vol. 49, pp. 2116–2125, 2013. [Online]. Available: <https://api.semanticscholar.org/CorpusID:13836038>
- [47] G. Pellegrino, B. Boazzo, and T. M. Jahns, “Magnetic model self-identification for pm synchronous machine drives,” *IEEE Transactions on Industry Applications*, vol. 51, no. 3, pp. 2246–2254, 2015.

Kishan Srinivasan received the B.Tech degree in electrical engineering from Pandit Deendayal Energy University, India in 2019 and MS degree from the University of Michigan, Ann Arbor in 2021, where he is currently pursuing the Ph.D. degree with the Department of Electrical Engineering and Computer Science. His research interests include power electronics, electric machines and drives.

Heath F. Hofmann (S’90–M’92–SM’16–F’22) received the Ph.D. degree in electrical engineering and computer science from the University of California at Berkeley, Berkeley, CA, USA, in 1998. He is currently a Professor with the University of Michigan, Ann Arbor, MI, USA. He has authored approximately five dozen papers in refereed journals, and currently holds 8 patents. His research interests include power electronics, specializing in the design, simulation, and control of electromechanical systems.

Jing Sun received the Ph.D. degree from the University of Southern California at Los Angeles, Los Angeles, CA, USA, in 1989. She is currently the Michael G. Parsons Collegiate Professor with the Department of Naval Architecture and Marine Engineering, with joint appointments with the Department of Electrical Engineering and Computer Science, and the Department of Mechanical Engineering, University of Michigan, Ann Arbor, MI, USA. Her research interests include modeling, control, and optimization of dynamic systems, with applications to marine and automotive systems. Dr. Sun is a fellow of the National Academy of Inventors, International Federation of Automatic Control (IFAC), and the Society of Naval Architects and Marine Engineers. She was a recipient of the 2003 IEEE Control System Technology Award.